Comparative Study of High-Resolution Shock-Capturing TVD Schemes

A. Sedaghat*, S. Shahpar†
The Manchester School of Engineering
Aerospace Engineering Division, Oxford Road
Manchester M13 9PL, England, UK

Abstract : A class of high-resolution shock-capturing schemes titled as Total Variation Diminishing (TVD) has been devised for numerical solution of multidimensional fluid dynamics problems by Yee [1]. These TVD schemes can be classified into symmetric and upwind schemes. The implementation and effects on accuracy of using different "limiters" with symmetric and upwind TVD schemes have been investigated and are reported in this article. The upwind approach proved to have slightly better shock -capturing capability for the two-dimensional shock reflection test problem that is considered here.

1. Introduction

Several newly developed high-resolution shock-capturing methods have been shown to be applicable to many multidimensional fluid dynamics problems for a perfect gas. For problems containing moderate to fairly strong shocks, these methods produce highly smooth solutions near discontinuities. These numerical methods belong to the class of Total Variation Diminishing (TVD) schemes. There exist many ways to achieve

*Research student.
†Research fellow in Aerospace Engineering.

higher-order spatial accuracy and at the same time have TVD-type properties. One way is due to Harten, Roe, and Yee referred to as the non-MUSCL approach [2].

It must be emphasized that the basic high-resolution shock-capturing methods for hyperbolic conservation laws were originally developed for nonlinear scalar hyperbolic conservation laws. Extension of scalar methods to nonlinear systems is accompolished by assuming certain physical models or by local linearization. The mathematical foundation relies mainly on the scalar case. There is no theory devised for nonlinear systems or for the multidimensional counterpart. These schemes are formally extended to one- or higher- dimensional nonlinear systems of hyperbolic conservation laws via the so-called Reimann solvers and are evaluated by numerical experiments.

There exist three popular ways of extending scalar schemes to nonlinear systems via the Reimann solver approaches: the exact Reimann solvers, the approximate Reimann solvers, and the flux-vector splitting techniques. The combination of the three Reimann solvers and of the differencing algorithms considered above yields five different scheme: a symmetric TVD scheme, an upwind TVD scheme, and three MUSCL-type schemes. In this work only non-MUSCL approaches have been considered.

2. Euler Equations

The equations of fluid flow without viscous forces, body forces, heat conduction or energy sources are referred to as the Euler equations. The Euler equations in two-dimensional Cartesian coordinates and in conservation-law form can be written as

$$\frac{\partial \mathbf{U}}{\partial t} + \frac{\partial \mathbf{F}(\mathbf{U})}{\partial x} + \frac{\partial \mathbf{G}(\mathbf{U})}{\partial y} = 0 \tag{1}$$

where

$$\mathbf{U} = \begin{bmatrix} \rho \\ \rho u \\ \rho v \\ e \end{bmatrix} \quad , \quad \mathbf{F} = \begin{bmatrix} \rho u \\ p + \rho u^2 \\ \rho uv \\ (e+p)u \end{bmatrix} \quad , \quad \mathbf{G} = \begin{bmatrix} \rho v \\ \rho uv \\ p + \rho v^2 \\ (e+p)v \end{bmatrix} \tag{2}$$

The primitive variables are the density ρ, the velocity components u and v, and the pressure p. The total energy per unit volume e, is related to p by,

$$p = (\gamma - 1)[e - \frac{1}{2}\rho(u^2 + v^2)] \tag{3}$$

where γ is the ratio of specific heats (γ= 1.4 for air).

The strong conservation-law form of Euler equations under a generalized coordinate transformation, $\xi = \xi(x,y)$ and $\eta = \eta(x,y)$, can be written as [2,3]

$$\frac{\partial \hat{\mathbf{U}}}{\partial t} + \frac{\partial \hat{\mathbf{F}}(\hat{\mathbf{U}})}{\partial \xi} + \frac{\partial \hat{\mathbf{G}}(\hat{\mathbf{U}})}{\partial \eta} = 0 \tag{4}$$

where

$$\begin{aligned} \hat{\mathbf{U}} &= \mathbf{U}/J \\ \hat{\mathbf{F}} &= (\xi_x \mathbf{F} + \xi_y \mathbf{G})/J \quad , \quad \hat{\mathbf{G}} = (\eta_x \mathbf{F} + \eta_y \mathbf{G})/J \\ J &= \xi_x \eta_y - \xi_y \eta_x \end{aligned} \tag{5}$$

where J is the Jacobian of the transformation. The Jacobian matrices $\hat{\mathbf{A}}$ and $\hat{\mathbf{B}}$ of $\hat{\mathbf{F}}$ and $\hat{\mathbf{G}}$ can be written as

$$\hat{\mathbf{A}} = \xi_x \mathbf{A} + \xi_y \mathbf{B} \quad , \quad \hat{\mathbf{B}} = \eta_x \mathbf{A} + \eta_y \mathbf{B}$$

where $\mathbf{A} = \partial \mathbf{F}/\partial U$ and $\mathbf{B} = \partial \mathbf{G}/\partial U$.

The eigenvalues of $\hat{\mathbf{A}}$ and $\hat{\mathbf{B}}$ are

$$\mathbf{a}_\mu = \begin{bmatrix} \mu_x u + \mu_y v - K_\mu c \\ \mu_x u + \mu_y v \\ \mu_x u + \mu_y v + K_\mu c \\ \mu_x u + \mu_y v \end{bmatrix} \tag{6}$$

where

$$\begin{aligned} \mu &= \xi \qquad for \quad \hat{\mathbf{A}} \\ \mu &= \eta \qquad for \quad \hat{\mathbf{B}} \end{aligned}$$

and

$$\begin{aligned} c &= \sqrt{\gamma P/\rho} \\ K_\mu &= \sqrt{\mu_x^2 + \mu_y^2} \end{aligned} \tag{7}$$

The x and y subscripts represent the partial derivatives with respect to x and y, whereas other subscripts simply refer to directions.

Furthermore, the matrix of the eigenvectors of $\hat{\mathbf{A}}$ and $\hat{\mathbf{B}}$, $\mathbf{R}_\mu = (R_\mu^1, R_\mu^2, R_\mu^3, R_\mu^4)$ can be written as

$$\mathbf{R}_\mu = \begin{bmatrix} 1 & 1 & 1 & 0 \\ u - K_{\mu 1} c & u & u + K_{\mu 1} c & K_{\mu 2} \\ v - K_{\mu 2} c & v & v + K_{\mu 2} c & K_{\mu 1} \\ H - K_{\mu 1} uc - K_{\mu 2} vc & \frac{u^2+v^2}{2} & H + K_{\mu 1} uc + K_{\mu 2} vc & K_{\mu 1} v + K_{\mu 2} c \end{bmatrix} \tag{8}$$

where

$$H = \frac{c^2}{\gamma - 1} + \frac{u^2 + v^2}{2} \tag{9}$$

and

$$K_{\mu 1} = \frac{\mu_x}{K_\mu} \quad , \quad K_{\mu 2} = \frac{\mu_y}{K_\mu} \tag{10}$$

3. Numerical Algorithm

The grid spacing is denoted by $\Delta\xi$ and $\Delta\eta$ such that $\xi = i\Delta\xi$ and $\eta = j\Delta\eta$, where $\Delta\xi$ and $\Delta\eta$ are constant increments in the ξ and η directions in the computational plane. Yee's explicit, second order accurate TVD scheme [1] can be implemented in two space dimensions by the method of time splitting as follows

$$\hat{\mathbf{U}}_{i,j}^{n+1} = L_\eta^h L_\xi^h \hat{\mathbf{U}}_{i,j}^n \tag{11}$$

$$\hat{\mathbf{U}}_{i,j}^{*} = L_\xi^h \hat{\mathbf{U}}_{i,j}^n = \hat{\mathbf{U}}_{i,j}^n - \frac{h}{\Delta\xi}(\tilde{\mathbf{F}}_{i+1/2,j}^n - \tilde{\mathbf{F}}_{i-1/2,j}^n) \tag{12}$$

$$\hat{\mathbf{U}}_{i,j}^{n+1} = L_\eta^h \hat{\mathbf{U}}_{i,j}^{*} = \hat{\mathbf{U}}_{i,j}^{*} - \frac{h}{\Delta\eta}(\tilde{\mathbf{G}}_{i,j+1/2}^{*} - \tilde{\mathbf{G}}_{i,j-1/2}^{*}) \tag{13}$$

with $h = \Delta t$. The numerical flux function $\tilde{\mathbf{F}}_{i+1/2,j}$ is expressed as

$$\tilde{\mathbf{F}}_{i+1/2} = \frac{1}{2}\left[\hat{\mathbf{F}}_i + \hat{\mathbf{F}}_{i+1} + (\mathbf{R}_{i+1/2}\mathbf{\Phi}_{i+1/2})/J_{i+1/2}\right] \tag{14}$$

The values of $(\xi_x)_{i+1/2}$, $J_{i+1/2}$, $(K_1)_{i+1/2}$, and $(K_2)_{i+1/2}$ in the $\xi-$direction can be determined by

$$J_{i+1/2} = \frac{1}{2}[J_i + J_{i+1}] \tag{15}$$

$$(\xi_x)_{i+1/2} = \frac{1}{2}[(\xi_x)_i + (\xi_x)_{i+1}] \tag{16}$$

$$(K_\xi)_{i+1/2} = \sqrt{(\xi_x)_{i+1/2}^2 + (\xi_y)_{i+1/2}^2} \tag{17}$$

and

$$(K_1)_{i+1/2} = \frac{(\xi_x)_{i+1/2}}{(K_\xi)_{i+1/2}} \tag{18}$$

$$(K_2)_{i+1/2} = \frac{(\xi_y)_{i+1/2}}{(K_\xi)_{i+1/2}} \tag{19}$$

The values ξ_x, ξ_y, η_x, and η_y can be determined by three-point central differences. $\mathbf{R}_{i+1/2}$ is determined from $\mathbf{U}_{i+1/2}$ which is computed by some symmetric average of $\mathbf{U}_i$ and $\mathbf{U}_{i+1}$, e.g. Roe's averaging. Similarly, one can define the numerical flux $\tilde{\mathbf{G}}_{j+1/2}$ in this manner.

3.1. Symmetric TVD Scheme

In a second-order symmetric TVD scheme, the elements of the $\Phi_{i+1/2}$ function in the $\xi-$direction denoted by $(\phi^l_{i+1/2})^S$ can be written as [5,6]

$$(\phi^l_{i+1/2})^S = -\lambda\beta(a^l_{i+1/2})^2 Q^l_{i+1/2} - \psi(a^l_{i+1/2})(\alpha^l_{i+1/2} - Q^l_{i+1/2}) \tag{20}$$

whereas for two-step TVD schemes it takes the form [7]

$$(\phi^l_{i+1/2})^S = -[\psi(\lambda a^l_{i+1/2}) - \beta(\lambda a^l_{i+1/2})^2](\alpha^l_{i+1/2} - Q^l_{i+1/2}) \tag{21}$$

The $Q^l_{i+1/2}$ is the limiter function and is described in the next section. $\alpha^l_{i+1/2}$ is the characteristic speed defined in (23) and is obtained from $U_{i+1/2}$.

Here, β is a parameter such that when it is equal to one, the method is best suited for time accurate calculations, and when it is equal to zero, it is mainly used for steady state applications [5], $a^l_{i+1/2}$ is the eigenvalue given by (6) and $\lambda = \Delta t/\Delta\xi$.

The function ψ is defined as

$$\psi(z) = \begin{cases} |z| & |z| \geq \epsilon \\ (z^2+\epsilon^2)/2\epsilon & |z| < \epsilon \end{cases} \tag{22}$$

The $\psi(z)$ function is an entropy correction to $|z|$ where ϵ is a small positive parameter and has the dimension of velocity. In practice the commonly used values [7] are in the range $0.05 \leq \epsilon \leq 0.2$. The $\alpha^l_{i+1/2}$ term is defined as

$$\alpha^l_{i+1/2} = R^{-1}_{i+1/2}(\hat{\mathbf{U}}_{i+1} - \hat{\mathbf{U}}_i) \tag{23}$$

3.2. Limiter Functions for Symmetric Schemes

Examples of limiter functions $Q^l_{i+1/2}$ for symmetric TVD schemes are [5,6]

$$\begin{aligned} Q^l_{i+1/2} &= minmod(\alpha^l_{i-1/2}, \alpha^l_{i+1/2}) + minmod(\alpha^l_{i+1/2}, \alpha^l_{i+3/2}) \\ &\quad -\alpha^l_{i+1/2} \qquad (24) \\ Q^l_{i+1/2} &= minmod(\alpha^l_{i-1/2}, \alpha^l_{i+1/2}, \alpha^l_{i+3/2}) \qquad (25) \\ Q^l_{i+1/2} &= minmod[2\alpha^l_{i-1/2}, 2\alpha^l_{i+1/2}, 2\alpha^l_{i+3/2} \\ &\quad , \ 1/2(\alpha^l_{i-1/2} + \alpha^l_{i+3/2})] \qquad (26) \end{aligned}$$

The above relations are later referred to as limiters 1, 2, and 3 respectively. The "minmod" function of a list of arguments is equal to the smallest number in absolute value if the list of arguments are of the same sign or is equal to zero if any two arguments are of the opposite sign. A suitable form of "minmod" function for inclusion in a computer code can be expressed as

$$\begin{aligned} minmod(a,b,c,\ldots,m) &= S.max\{0, min[|a|, S.b, S.c, \ldots, S.m]\} \quad (27) \\ S &= sign(1,a) \quad (28) \end{aligned}$$

3.3. Upwind TVD Scheme

The elements of the $\Phi_{i+1/2}$ denoted by $(\phi^l_{i+1/2})^U$ for the second-order upwind TVD scheme, originally developed by Harten [8] and later modified and generalized by Yee [5,6], are

$$(\phi^l_{i+1/2})^U = \sigma(a^l_{i+1/2})(g^l_{i+1} + g^l_i) - \psi(a^l_{i+1/2} + \gamma^l_{i+1/2})\alpha^l_{i+1/2} \quad (29)$$

with the function $\sigma(z)$ as [5]

$$\sigma(z) = \frac{1}{2}[\psi(z) - \beta\lambda z^2] \quad (30)$$

and

$$\gamma^l_{i+1/2} = \sigma(a^l_{i+1/2}) \begin{cases} (g^l_{i+1} - g^l_i)/\alpha^l_{i+1/2} & \alpha^l_{i+1/2} \neq 0 \\ 0 & \alpha^l_{i+1/2} = 0 \end{cases} \quad (31)$$

where $a^l_{i+1/2}$, $\alpha^l_{i+1/2}$, and ψ are the same as those given for symmetric TVD scheme.

3.4. Limiter Functions for Upwind Schemes

Examples of limiter functions $Q^l_{i+1/2}$ suitable for the upwind TVD scheme outlined above are given in [5,6] and are as follows,

$$\begin{aligned} g^l_i &= minmod(\alpha^l_{i-1/2}, \alpha^l_{i+1/2}) \quad (32) \\ g^l_i &= (\alpha^l_{i+1/2}\alpha^l_{i-1/2} + |\alpha^l_{i+1/2}\alpha^l_{i-1/2}|)/(\alpha^l_{i-1/2} + \alpha^l_{i+1/2}) \quad (33) \\ g^l_i &= S.max\{0, min[2\ |\alpha^l_{i+1/2}|, S\alpha^l_{i-1/2}], min[|\alpha^l_{i+1/2}|, 2\ S\alpha^l_{i-1/2}]\} \quad (34) \\ g^l_i &= \{\alpha^l_{i-1/2}[(\alpha^l_{i+1/2})^2 + \delta] + \alpha^l_{i+1/2}[(\alpha^l_{i-1/2})^2 + \delta]\} \\ &\quad /[(\alpha^l_{i+1/2})^2 + (\alpha^l_{i-1/2})^2 + 2\delta] \quad (35) \end{aligned}$$

where $S = sign(1, \alpha^l_{i+1/2})$ and δ is a small parameter. In practice, the commonly used range [7] for δ is quoted to be $10^{-7} \leq \delta \leq 10^{-5}$.

The above relations are later referred to as limiters 1, 2, 3, and 4 respectively.

3.5. Roe's Averaging

One method of finding variables at cell faces e.g. $(i+1/2, j+1/2)$ etc. is given by Roe [9]. For two-dimensional flows Roe's averaging can be written as

$$u_{i+1/2,j} = \frac{bu_{i+1,j} + u_{i,j}}{b+1} \tag{36}$$

$$v_{i+1/2,j} = \frac{bv_{i+1,j} + v_{i,j}}{b+1} \tag{37}$$

$$H_{i+1/2,j} = \frac{bH_{i+1,j} + H_{i,j}}{b+1} \tag{38}$$

$$c^2_{i+1/2,j} = (\gamma-1)[H_{i+1/2,j} - \frac{1}{2}(u^2_{i+1/2,j} + v^2_{i+1/2,j})] \tag{39}$$

where

$$b = \sqrt{\rho_{i+1,j}/\rho_{i,j}} \tag{40}$$

and c is the local speed of sound. The total enthalpy H is given by (9).

3.6. Stability of the Solution

The stability condition can be related to the Courant number for time splitting schemes. For two-dimensional flow in general coordinates the Courant number can be determined from

$$b_\xi = max_{i,j}(\mid \hat{u_x} \mid + K_\xi c)/\Delta\xi \tag{41}$$

$$b_\eta = max_{i,j}(\mid \hat{u_y} \mid + K_\eta c)/\Delta\eta \tag{42}$$

$$\nu = \Delta t.max(b_\xi, b_\eta) \quad , \quad \nu \leq 1 \tag{43}$$

where

$$\hat{u_x} = \xi_x u + \xi_y v \tag{44}$$

$$\hat{u_y} = \eta_x u + \eta_y v \tag{45}$$

and

$$K_\xi = \sqrt{\xi_x^2 + \xi_y^2} \tag{46}$$

$$K_\eta = \sqrt{\eta_x^2 + \eta_y^2} \tag{47}$$

4. Shock Reflection Test Case

In order to examine the ability of the TVD schemes, a supersonic flow over a flat plate is considered here. The effects of using different limiters for symmetric and upwind TVD schemes have been investigated. The time-accurate mode $\beta = 1$ has been used for this case.

In the numerical experiments, a shock angle of $\beta = 29°$ and a free stream Mach number(M_∞) of 2.9 are used. The computational region is bounded by $0 \leq x \leq 4.1$, and $0 \leq y \leq 1$. The computational grid consists of 63×23 mesh points.

The entire flow field is initially set equal to the free stream supersonic inflow values. In addition, the following boundary conditions are used: a) supersonic inflow, b) specified shock angle and shock strength for the upper boundary, c) rigid flat plate for the lower boundary, and d) supersonic outflow.

Defining $\mathbf{U}_{i,j} = [u_{1,i,j}, u_{2,i,j}, u_{3,i,j}, u_{4,i,j}]^T$ the numerical boundary condition on the rigid surface is written by using a second-order one sided approximation for $\partial P/\partial y$ plus v=0 on the wall at $j = 2$ as follows

$$\begin{aligned} u_{1,i,1} &= u_{1,i,3} \quad , \quad u_{1,i,2} = u_{1,i,3} \\ u_{2,i,1} &= u_{2,i,3} \quad , \quad u_{2,i,2} = u_{2,i,3} \\ u_{3,i,1} &= -u_{3,i,3} \quad , \quad u_{3,i,2} = 0 \\ u_{4,i,1} &= u_{4,i,3} \end{aligned} \tag{48}$$

The term $u_{4,i,2}$ is determined as follows

$$P_{i,2} = (4\ P_{i,3} - P_{i,4})/3 \quad , \quad u_{4,i,2} = \frac{P_{i,2}}{(\gamma - 1)} + \frac{u_{i,3}^2}{2\rho_{i,3}} \tag{49}$$

Since TVD schemes are five-point stencil in each coordinate directions, values of limiters ,e.g. an upwind limiter g_i^l, are needed to be estimated at boundaries. Three ways of obtaining g_i^l at boundaries are discussed in [5], which for lower boundary (i=1) are as follows

$$g_1^l = 0 \quad , \quad g_1^l = g_2^l \quad , \quad g_1^l = \alpha_{3/2} \tag{50}$$

However, in the present computation the following relations are used

$$g_1^l = g_2^l \quad , \quad g_2^l = \alpha_{3/2} \tag{51}$$

which leads to $(\mathbf{R\Phi})_{3/2}$ to be zero at boundaries. Note that symmetric schemes are insensitive to this correction; therefore, the same terminology has been applied at boundaries, i.e. $(\mathbf{R\Phi})_{3/2} = 0$.

The ϵ in Eq. (11) is set equal to 0.1 for all test cases.

5. NACA0012 Aerofoil Test Case

The NACA0012 aerofoil has been selected to examine the ability of the TVD schemes in curvilinear coordinates. The computational grid consists of 71×21 C-type mesh, see Fig. 2e. The meshes have been clustered near to the surface in order to simulate similar meshes as used for Navier-Stokes computations. A transonic flow $M_\infty = 0.8$ at zero incidence ($\alpha = 0$) is considered here. The effects of using different limiters for symmetric and upwind TVD schemes have been investigated. Local time-stepping and $\beta = 0$ has been used for this case.

The following boundary conditions are used for this test case: a) Charasteristic [10] boundary conditions are used at the outer bondaries; b) Velocity at next adjecent point to the surface is rotated as to be tangential to the surface and applied on the surface; c) Zero normal pressure gradient is used to evaluate pressure on the surface; d) To find density at the aerofoil surface, total enthalpy on the surface is fixed to be equals to the freestream total enthalpy; and e) A simple averaging is used to evaluate conservative varaibles at cut in the wake region.

Limiters have been corrected at boundaries similar as the shock-reflection test case.

6. Discussion of Numerical Results

Shock Reflection Test Case . All of the computations for the two-dimensional shock-reflection problem were done in single precision using a HP700 computer. It took 350 time step iterations to obtain converged solutions for the uniform grids with a fixed Courant number of $\nu = 0.8$. Results for the shock-reflection test case are presented in Fig. 1. Pressure coefficient distribution at middle of computational domain (j=12) and convergence history based on Root Mean Square (RMS) are presented for both symmetric and upwind TVD schemes. Based on sharp prediction of shock wave position and smooth convergence, the limiter 2 for symmetric scheme and the limiter 3 for upwind scheme are preferable over the other limiters. The results corespond to the upwind scheme indicate sharper prediction for shock wave position compare with the symmetric TVD scheme. Forty pressure contours between the maximum and minimum values are shown for the upwind TVD scheme in Fig. 1e. The limiter 3 is used here.

NACA0012 Aerofoil Test Case . Results for the NACA0012 aero-

foil test case are presented in Fig. 2 for symmetric TVD scheme and in Fig. 3 for upwind TVD scheme. Surface pressure coefficient, drag convergence, surface entropy change $\Delta s = \frac{p/\rho^{\gamma}}{s_{\infty}} - 1$, and convergence history are presented in Fig. 2a, 2b, 2c, 2d for symmetric method and in Fig. 3a, 3b, 3c, 3d for upwind method, respectively. Results correspond to all limiters except for upwind scheme which the limiter 4 failed to produce some results. The computational mesh is presented in Fig. 2e and the pressure contours corresponds to the best limiter (upwind with limiter 3) are presented in Fig. 3e.

Effects of different limiters on final results are more observable for this test case. Shock wave position is suppoed to be at $x = 0.5$ as reported from other theoritical and numerical results [11]. For symmetric TVD schemes, relatively right shock wave position was obtained using the limiters 2 and 3 . Drag coefficient and entropy difference were overpredicted using all limiters. The right value of C_D is reported to be in the range of $0.008 - 0.01$ on reference [11]. In theory, entropy difference must be zero before shock wave and then has a jump after it. But, all numerical schemes generate entropy and a good mesearment on accuracy of numerical schemes can be lower prediction of entropy difference. The lowest value for entropy difference corresponds to limiter 3. From convergence behaviour of the scheme using different limiters, the limiter 3 was found to be the best choice for this scheme. In overal, comparing results correspond to symmetric scheme with upwind scheme, it is found that the best results are obtained using upwind TVD scheme with limiter 3 (look at Fig. 3). However, limiter 2 can also be counted as a good limiter in finer meshs for this scheme.

7. Conclusion

Upwind and Symmetric TVD schemes are presented in general coordinates for two-dimensional problems. Numerical results show that the upwind TVD schemes can produce more accurate solutions than symmetric TVD schemes in a relatively coarse meshes. Limiters have important role on accuracy of final results. It has shown that the most robust results can be achieved by using the limiter 3 (Van-Leer limiter) corresponds to the upwind TVD schemes. The extension of these schemes to compute complex problems e.g. viscous turbulent flows over transonic porous aerofoils is the subject of current research.

References

[1] Yee, H. C. and Warming, R. F., 'Implicit Total Variation Diminishing (TVD) Schemes for Steady-State Calculations' AIAA Paper

No. 83-1902, Proc. of the AIAA 6th Computational Fluid Dynamics Conference, Danvers, Mass., July 1983.

[2] Yee, H. C., and Kutler, P., 'Application of Second-Order Accurate Total Variation Diminishing (TVD) Schemes to the Euler Equations in General Geometries', NASA TM-85845, Ames Research Centre, Moffett Field, CA, August 1983.

[3] Yee, H. C., Klopfer, G. H., Montagne, J. L., 'High Resolution Shock-Capturing Schemes for Inviscid and Viscous Hypersonic Flows', J. Comp. Phys., vol., pp 31-61, 1990.

[4] Hughson, M. C. and Beran, P. S., 'Analysis of Hypersonic Blunt-Body Flows Using a Total Variation Diminishing (TVD) Scheme and the MacCormack Scheme', AIAA 91-3206-CP, 1991.

[5] Yee, H. C., 'Upwind and Symmetric Shock-Capturing Schemes', NASA TM-89464, May 1987.

[6] Montagne, J. L. and Yee, H. C., 'Comparative Study of High-Resolution Shock-Capturing Schemes for a Real Gas', AIAA Journal, vol. 27, No. 10,pp 1332-1346, 1988.

[7] Yee, H. C. and Shinn, J. L., 'Semi-Implicit and Fully Implicit Shock-Capturing Methods for Hyperbolic Conservation Laws with Stiff Source Terms', AIAA 87-1116 CP, 1987.

[8] Harten, A., 'High Resolution Scheme for Hyperbolic Conservation Laws', J. Comp. Phys. 49, pp 357-393, 1983.

[9] Roe, P. L., 'Approximate Reimann Solvers, Parameter Vectors, and Difference Schemes', J. Comp. Phys., vol. 43, pp 357-372, 1983.

[10] Jameson, A. and Baker, T. J., 'Solution of the Euler Equations for Complex Configurations', AIAA Paper No. 83-1929, 1983.

[11] Rizzi, A. and Vivand H., 'Numerical Methods for the Computation of of Inviscid Transonic Flows with Shock Waves', Notes on Numerical Fluid Mechanics , Vol 3, Vieweg, 1981.

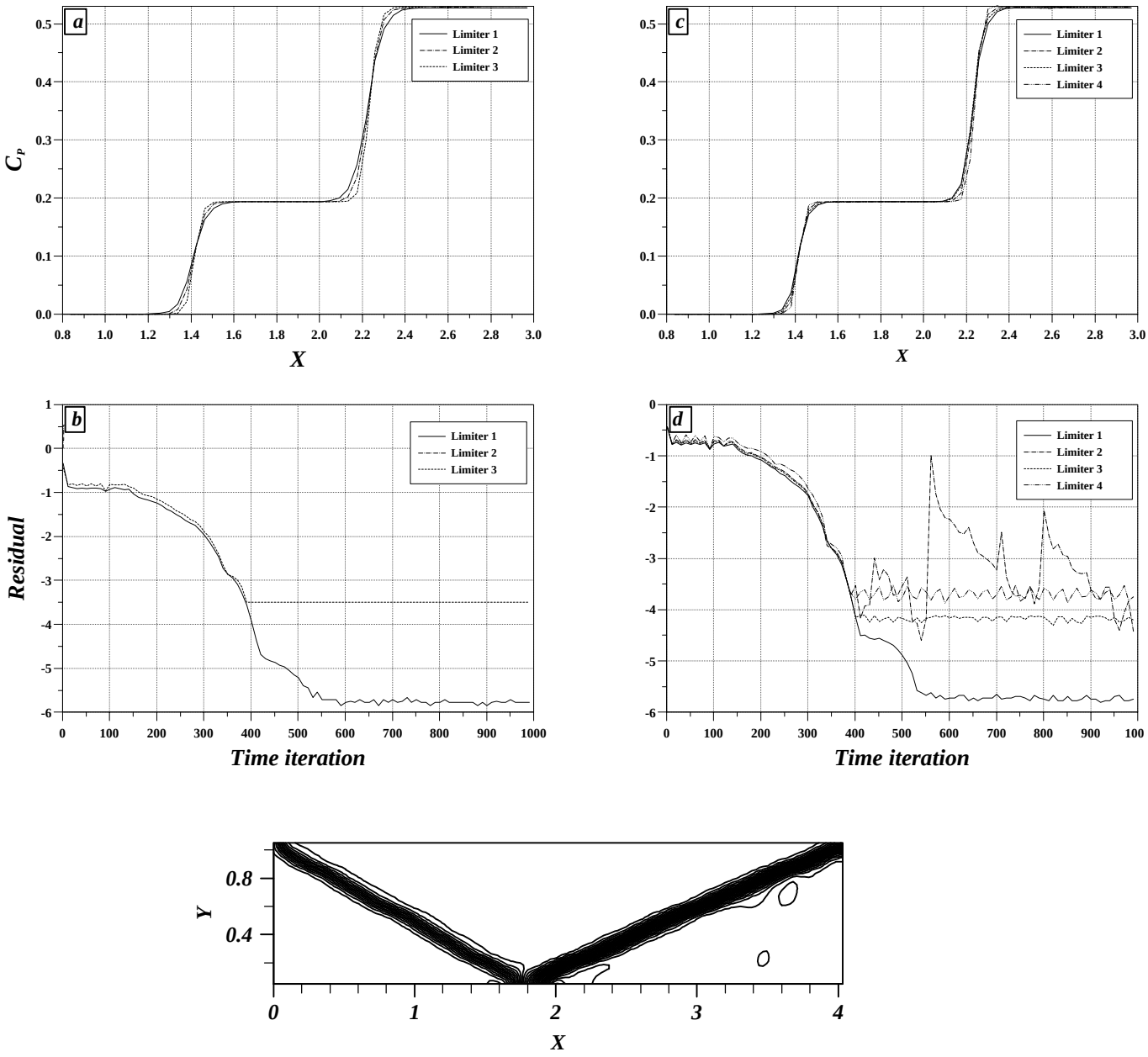

Figure 1: Results for shock-reflection over a flat plate. (a) Pressure coefficient at middle of domain, (b) convergence history using symmetric TVD scheme.(c) Pressure coefficient at middle of domain, (d) convergence history using upwind TVD scheme. (e) pressure contours corresponds to upwind TVD scheme using limiter 3.

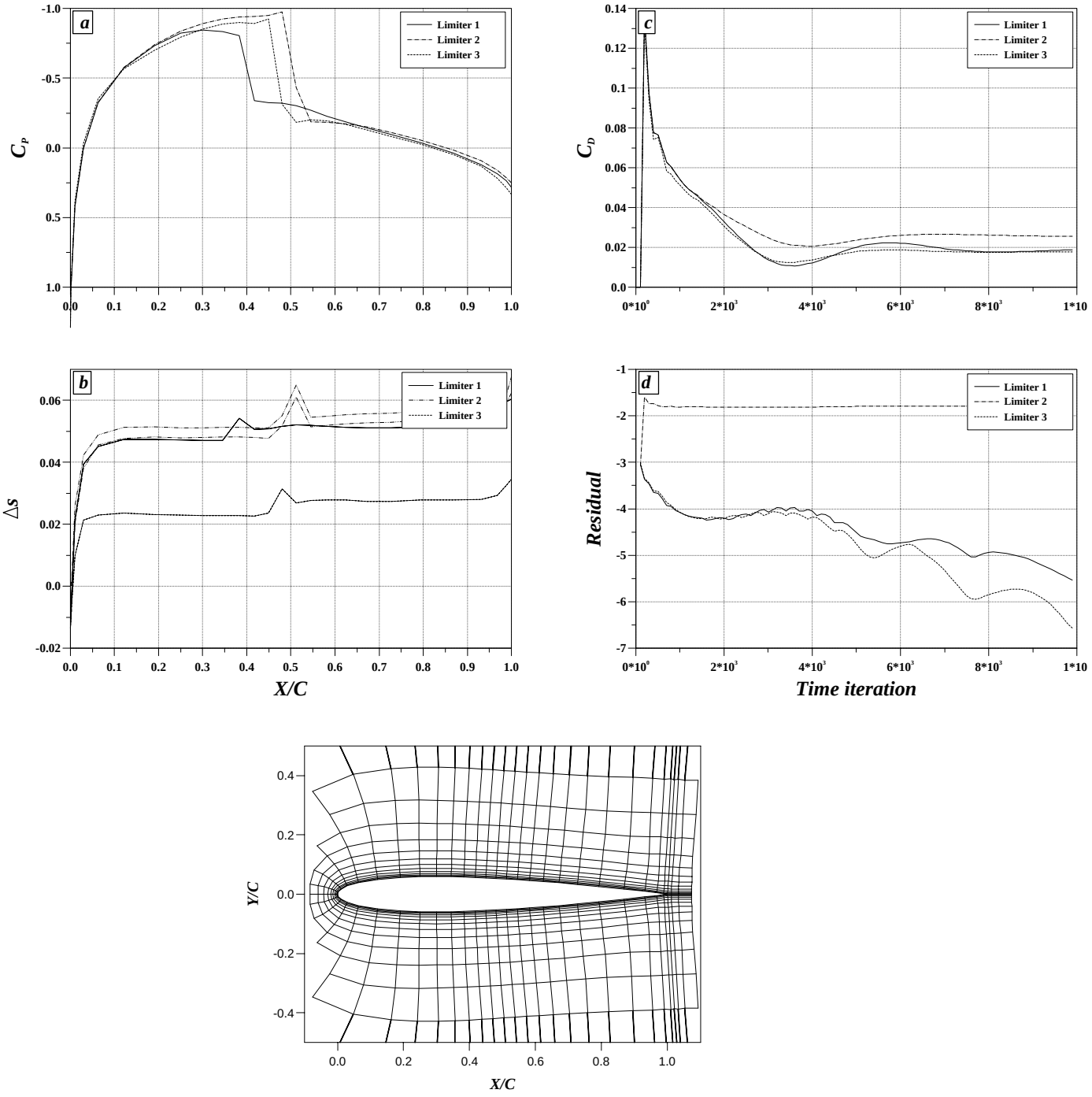

Figure 2: Results for the NACA0012 aerofoil at $M_\infty = 0.8$, $\alpha = 0$ using symmetric TVD scheme. (a) Surface pressure coefficient, (b) Drag convergence history, (c) Surface entropy difference, (d) Convergence history, and (e) Sectional view of C-hyperbolic mesh around the NACA0012 aerofoil.

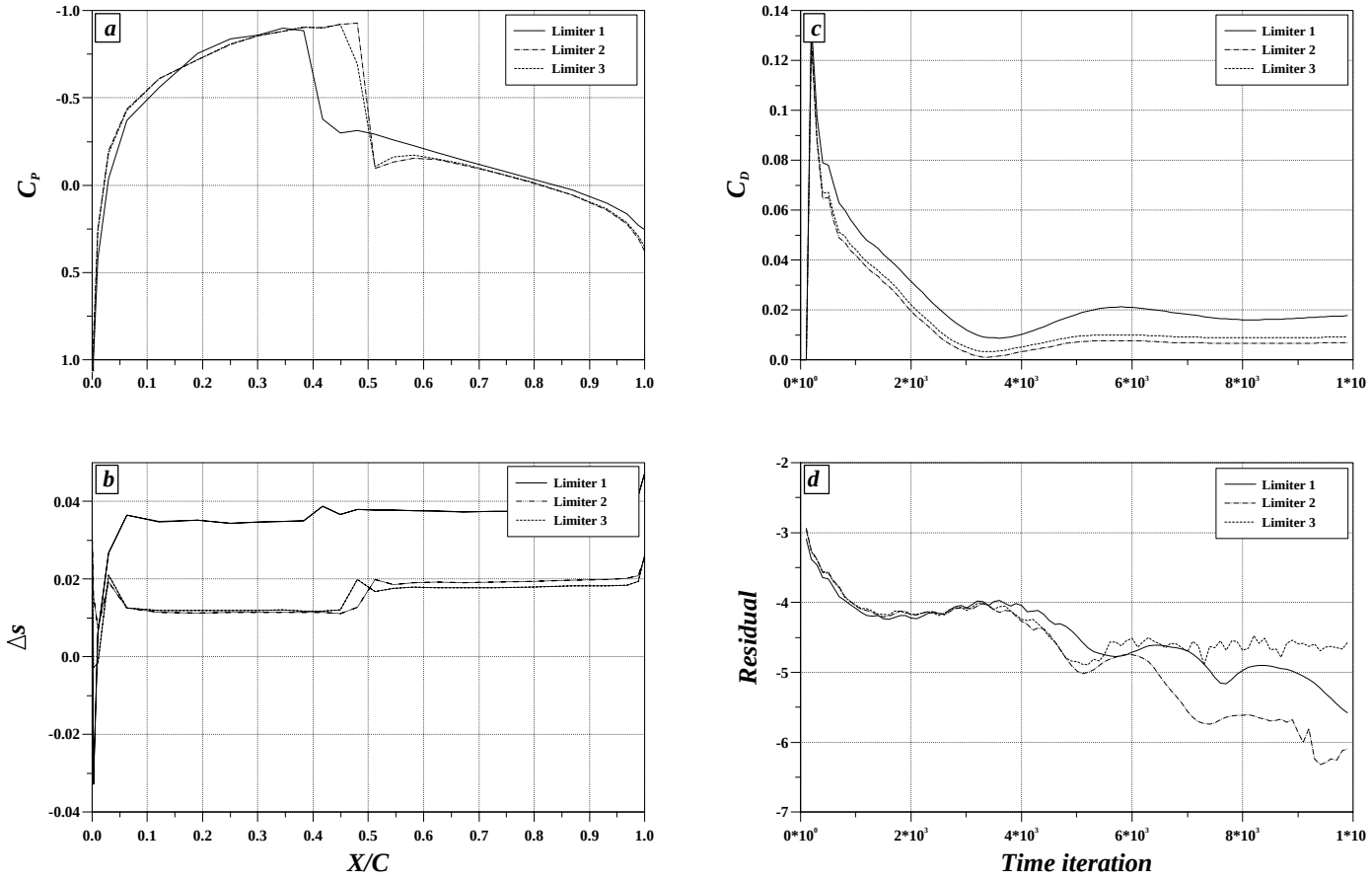

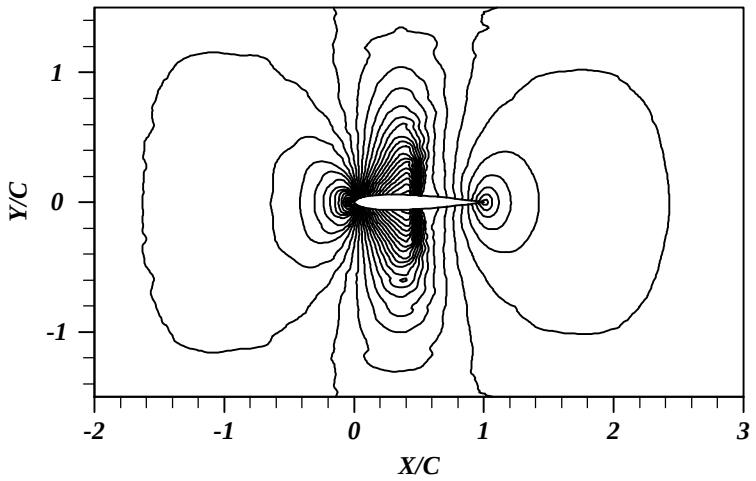

Figure 3: Results for the NACA0012 aerofoil at $M_\infty = 0.8$, $\alpha = 0$ using upwind TVD scheme. (a) Surface pressure coefficient, (b) Drag convergence history, (c) Surface entropy difference, (d) Convergence history, and (e) Pressure contours corresponds to upwind TVD scheme using limiter 3.